Monatsh Chem (2014) 145:97–101
DOI 10.1007/s00706-013-0980-0

ORIGINAL PAPER

Ab initio investigation of amorphous Sb_2Te

Wei Zhang · Ider Ronneberger · Yan Li · Riccardo Mazzarello

Received: 21 February 2013 / Accepted: 19 March 2013 / Published online: 15 May 2013

Abstract Chalcogenide phase-change alloys are an important class of materials for applications in data storage. In this work, we investigate the structural properties of the amorphous phase of the phase-change material Sb_2Te. We show that all the atoms in Sb_2Te are in a defective octahedral environment, that the majority of primitive rings are five- and four-membered, and that the voids are small and amount to about 2 % of the total volume of the system.

Keywords Ab initio calculations · Molecular dynamics · Kinetics · Phase transformations · Chalcogenides · Phase-change materials

Introduction

Phase-change materials (PCMs) are chalcogenide-based alloys that are capable of switching rapidly and reversibly between the amorphous and crystalline phases upon heating. The marked optical and electrical contrast between the two phases and the thermal stability of PCMs at room temperature has led to their application in data-storage devices, including rewritable optical media (CDs, DVDs, Blu-ray discs) and electronic nonvolatile memory (PC-RAM) [1, 2]. In these two classes of devices, heating is induced by laser irradiation and the Joule effect, respectively. Recent developments include the realization of PCM prototype devices displaying neuron-like processing capabilities [3], and the observation of magnetic contrast in PCMs doped with magnetic impurities [4–6]. Two classes of PCMs have proven to be the best candidates for practical applications: GeTe–Sb_2Te_3 pseudobinary alloys (group 1) and doped Sb–Te compounds near the eutectic composition $Sb_{70}Te_{30}$ (group 2). The structural and electronic properties of the crystalline and amorphous phases of these PCMs have been extensively studied experimentally [7–14]. There have also been numerous density functional theory (DFT) investigations of the crystalline phases of both groups of PCMs and the amorphous phases of group 1 materials [14–22]. However, only a few computational studies of amorphous group 2 PCMs have been performed [14].

The crystallization speeds of $Sb_{70}Te_{30}$ and other SbTe alloys, including Sb_2Te and Sb_4Te, are very high; however, their crystallization temperatures are relatively low (80–100 °C), which prevents their utilization in devices. The crystallization temperature can be significantly increased by doping with selected elements such as Ag, In, Ge, and Ga [23]. In [14], a Sb_4Te alloy doped with Ag and In, $Ag_{3.5}In_{3.8}Sb_{75.0}Te_{17.7}$ (AIST), was investigated using a combined experimental and DFT approach. It was shown that, just as it is in the crystalline phase, the local environment around Sb atoms in amorphous AIST is a 3 + 3 (distorted) octahedron. It was also suggested that fast crystallization occurs due to interchanges between short and long bonds. These results indicate that AIST behaves differently from most group 1 PCMs, in which the short-range order changes considerably upon amorphization [15–17, 19].

In the work described in the present paper, we performed ab initio molecular dynamics (AIMD) simulations to study the structural properties of clean amorphous Sb_2Te (a-Sb_2Te). Here, we compare the results of those simulations with the results of the previous work on AIST mentioned above [14], and discuss how the presence of Ag

W. Zhang · I. Ronneberger · Y. Li · R. Mazzarello (✉)
Institute for Theoretical Solid State Physics, JARA-FIT and JARA-HPC, RWTH Aachen University, Aachen, Germany
e-mail: mazzarello@physik.rwth-aachen.de

and In impurities and changes in the Sb concentration affect the short-range and medium-range order of the amorphous phase. In order to gain a better understanding, we also studied amorphous Sb_2Te_3 (a-Sb_2Te_3), an Sb–Te alloy that belongs to group 1 [24].

Results and discussion

We calculated the total $g(r)$ and the partial pair-correlation functions (PPCFs) based on the MD trajectory at 300 K (see Fig. 1).

In the case of a-Sb_2Te, the first peak in the Sb–Te and Sb–Sb PPCFs is around 2.95 Å, whereas the Te–Te PPCF shows no peak below 3.3 Å. This indicates that Te–Te bonds are absent, in agreement with the case of AIST [14]. The similar heights and widths of the first peaks in the Sb–Sb and Sb–Te PPCFs suggest that comparable amounts of heteropolar Sb–Te and homopolar Sb–Sb bonds are present. In the case of the Te-rich alloy Sb_2Te_3, on the other hand, the heteropolar Sb–Te bonds are prevalent, whereas the fraction of Te–Te bonds is relatively small. In a-Sb_2Te_3, there is also a significant fraction of Sb–Sb bonds, albeit much smaller than in a-Sb_2Te. In the total $g(r)$ of a-Sb_2Te_3, a tiny shift of the first peak to smaller distances is observed as compared to the $g(r)$ of a-Sb_2Te. For both compounds, the position of the first peak of the $g(r)$ is slightly shifted (about 3 %) to shorter r with respect to the $g(r)$ of the corresponding crystalline phases [25]. The $g(r)$ of crystalline Sb_2Te and that of Sb_2Te_3 exhibit a second peak at 3.2–3.3 Å, which reflects the existence of longer bonds and 3 + 3 distorted octahedral structures due to Peierls distortion. Matsunaga et al. [14] observed a shoulder on the second peak in the total correlation function of amorphous AIST, which corresponded to the second peak of the crystal, suggesting the existence of 3 + 3 octahedral structures in the disordered phase as well. However, we did not see any such feature in the total $g(r)$ and the PPCFs of our model of a-Sb_2Te. This might be due to the different stoichiometry (in particular, the lower concentration of Sb atoms in our model), or to the fact that their structure was refined using a reverse Monte Carlo method. It is interesting to note that, in the case of several group 1 PCMs such as GeTe and $Ge_2Sb_2Te_5$, much larger reductions in the average bond lengths occur upon amorphization [26].

Using the cutoff radius indicated in Fig. 1, we calculated the coordination numbers in both models. The distribution of the coordination numbers is shown in Fig. 2 and the average coordination numbers are presented in Table 1. In a-Sb_2Te, the majority of the Sb atoms are fourfold coordinated. The number of threefold- and fivefold-coordinated Sb atoms is quite large too. Te atoms have predominantly threefold or fourfold coordination, although a significant number of twofold-coordinated Te atoms are also present. While, in principle, there is no reason to expect a perfect agreement between our model and that for AIST provided in [14] given their different stoichiometries and the absence of impurities in our model, it turns out that the apparent discrepancies in the average coordination numbers of the

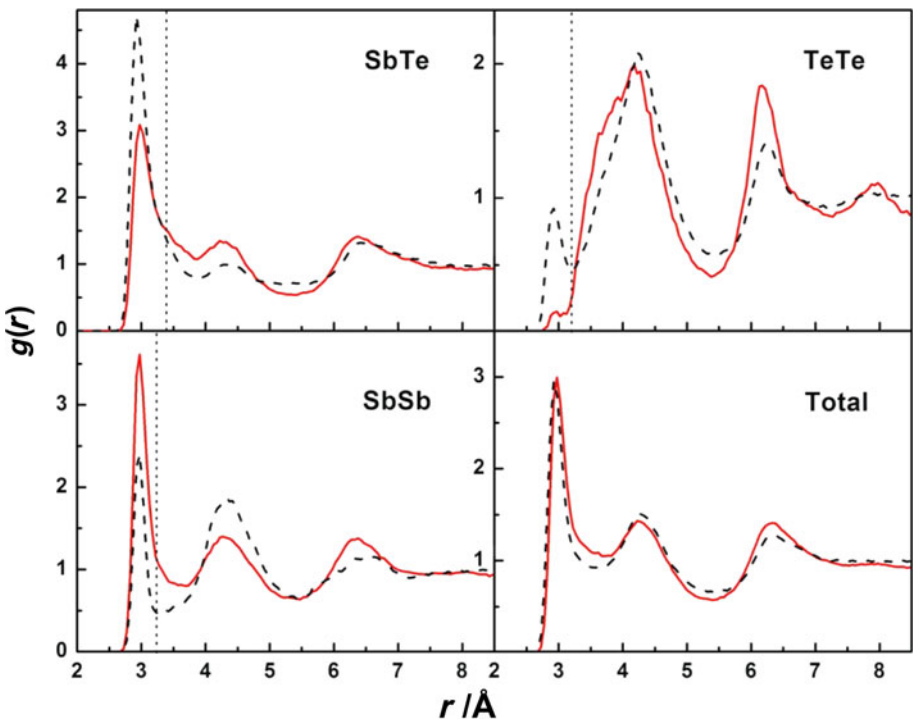

Fig. 1 Total and partial pair-correlation functions of amorphous Sb_2Te (*red solid line*) and Sb_2Te_3 (*black dashed line*) at 300 K. *Vertical lines* indicate the cutoff radius used to compute coordination numbers

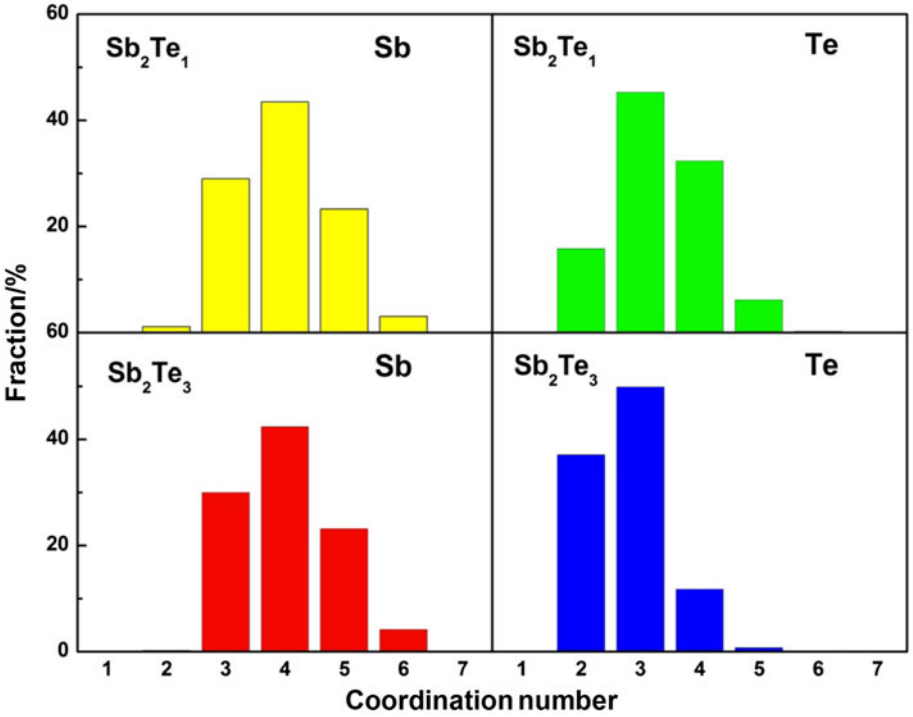

Fig. 2 Distributions of coordination numbers in amorphous Sb_2Te and Sb_2Te_3

Table 1 Average coordination numbers of Sb and Te atoms in amorphous Sb_2Te and (in parentheses) in Sb_2Te_3

	Total	Sb	Te
Sb	4.098 (4.111)	2.434 (0.721)	1.664 (3.390)
Te	3.394 (2.825)	3.322 (2.254)	0.072 (0.571)

Sb and Te atoms in the two models (see Table I in [14]) are mostly due to the larger cutoff radii used in our work. In a-Sb_2Te_3, the fraction of four-coordinated Sb atoms is larger than it is in a-Sb_2Te, and Te atoms are mostly two- and three-coordinated. In contrast to the case of a-Sb_2Te, the number of four-coordinated Te atoms is small. The latter results are in good agreement with those presented in [24].

The local order parameter q [15] was computed for each atom in the two models, and the results indicated that no tetrahedral structure was present. To shed light on the local bonding environment, we also calculated angular distribution functions. In Fig. 3, we show the angular distribution functions averaged over all atoms (black curve), over all Sb atoms (red curve), and over all Te atoms (blue curve) for both a-Sb_2Te and a-Sb_2Te_3. The distributions exhibit a large peak at $\sim 90°$ and a smaller peak at $\sim 165°$, indicating that most atoms are in a (defective) octahedral-like environment in both systems. In the case of a-Sb_2Te_3, there is no peak in the distribution function of Te near 180°, consistent with the fact that most Te atoms have a twofold or threefold coordination—without neighbors on opposite sides. In a-Sb_2Te, the number of Te atoms in a fourfold defective octahedral configuration is larger (see Fig. 2), hence a broad shoulder appears at large angles in the corresponding angular distribution function. In summary, the amorphous networks in a-Sb_2Te and a-Sb_2Te_3 mostly comprise defective octahedral motifs. A snapshot of the amorphous structure of a-Sb_2Te is shown in Fig. 4, where the most predominant structural motifs are represented by balls and sticks.

The distribution of primitive rings, which describes the medium-range order in the amorphous network, is shown in Fig. 5 for both systems. For a-Sb_2Te_3, four-membered rings are prevalent (18 %), in agreement with [24], whereas five-membered rings are the most common in the model of a-Sb_2Te (18 %), though the number of four-membered rings is only slightly smaller (15 %). Similar results hold for AIST [14]. The majority of the four-membered rings in a-Sb_2Te_3 (82 %) have SbTeSbTe alternation. This is not the case in a-Sb_2Te (25 %). In a-Sb_2Te, the fraction of larger rings (between six- and 14-membered) is quite significant. Interestingly, in a-Sb_2Te_3 the distribution of rings is even broader, and several very large rings are present. This result is in line with the low average coordination number of Te atoms in a-Sb_2Te_3.

We also calculated the volume occupied by cavities in the two amorphous systems using the method developed in [27], which is implemented in the program VNP [28]. Atomic radii are set equal to 50 % of the average bond length for each species, whereas the radius of the test

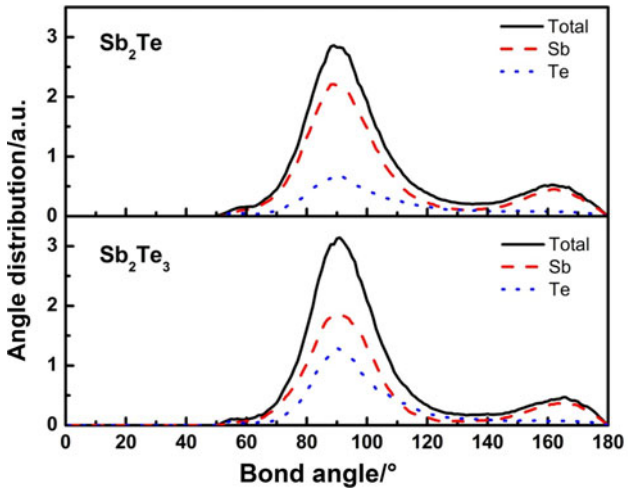

Fig. 3 Angle distribution functions of amorphous Sb_2Te and Sb_2Te_3

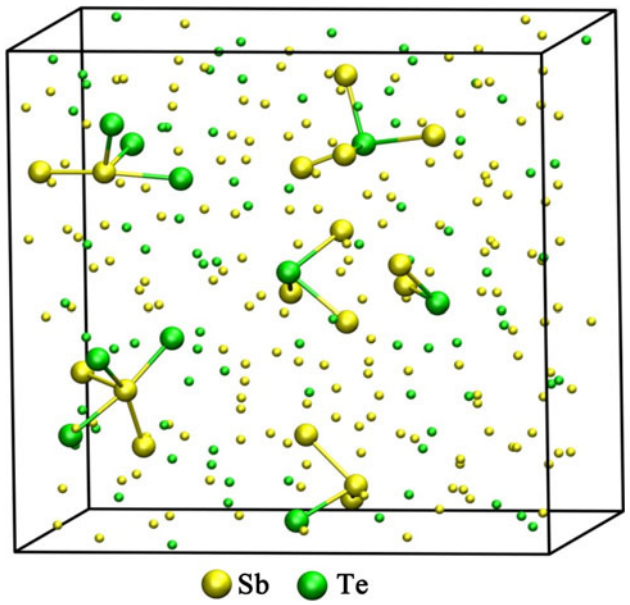

Fig. 4 Snapshot of amorphous Sb_2Te. The most common structural motifs are represented by balls and sticks

sphere is set to 1.3 Å. The fraction of the total volume occupied by the voids is 18 % in a-Sb_2Te_3 and 2 % in a-Sb_2Te. Furthermore, we computed the distribution of the volume of the cavities for the two amorphous systems (see Fig. 6). In agreement with [24], we found that the number of cavities in a-Sb_2Te_3 is large, as is their average size. On the other hand, there are only a few cavities in a-Sb_2Te, and they are small. The large concentration of voids and large rings in a-Sb_2Te_3 may be partly due to the fact that, for this system, we used the theoretical value for the density computed in [24] (we used an experimental one for a-Sb_2Te instead see "Methods"). Nevertheless, these results clearly indicate a more open structure in a-Sb_2Te_3.

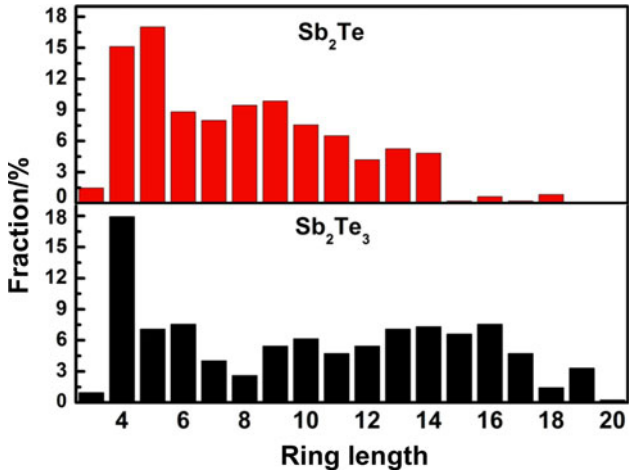

Fig. 5 Statistics for primitive rings in amorphous Sb_2Te and Sb_2Te_3 (*ring length* is the number of atoms in the ring)

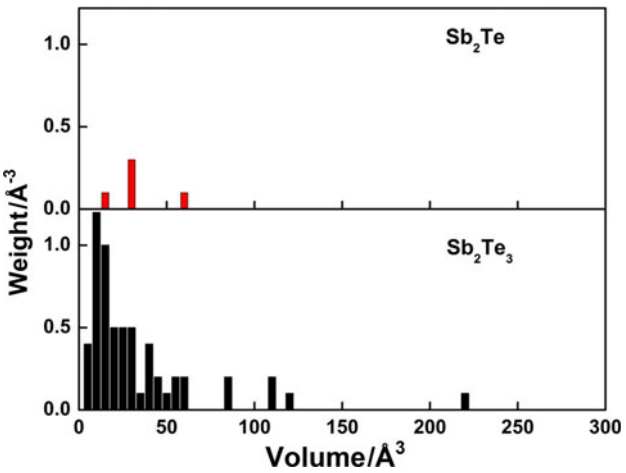

Fig. 6 Distributions of cavity volume for amorphous Sb_2Te and Sb_2Te_3

In conclusion, our study shows that amorphous Sb_2Te mostly consists of defective octahedral structures, as also seen in the case of Sb_2Te_3. In contrast to the latter, however, a-Sb_2Te has a less open structure, as evidenced by the smaller number of large rings and cavities.

Methods

The amorphous phases of both Sb_2Te and Sb_2Te_3 were generated by quenching from the melt. A novel, Car–Parrinello-like scheme [29] was adopted for our AIMD simulations. This method was implemented in the CP2K suite of programs [30, 31]. The generalized gradient approximation (GGA) to the exchange–correlation potential [32] and scalar-relativistic Goedecker pseudopotentials [33] were used. The Kohn–Sham orbitals were expanded in

a triple-zeta plus polarization Gaussian-type basis set, whereas the charge density was expanded in plane waves with a cutoff of 300 Ry. 270-atom models were considered for both alloys. Because of the large sizes of the models, the Brillouin zone was sampled at the Γ point only. The time step for the simulations was 2 fs. The systems were first randomized at very high temperature (3,000 K) for 14 ps, and then equilibrated at the (experimental) melting temperature for 30 ps, quenched from the melting temperature to 300 K within 30 ps, equilibrated at 300 K for 30 ps, and finally quenched to 10 K in 20 ps. Geometry optimization was also performed, starting from the low-temperature MD trajectory. The atomic density of Sb_2Te was set to the experimental value of 0.0309 atoms/Å^3 (we used the atomic density of Sb_2Te doped with Ag and In, as determined in [13], thereby assuming that the small amount of Ag and In does not change the atomic density significantly). Due to the lack of experimental data on the density of Sb_2Te_3, we used the theoretical value of 0.0271 atoms/Å^3, as determined in [24].

Acknowledgments We are grateful for discussions with P. Zalden, M. Salinga, and M. Wuttig. We also acknowledge the access provided to the computational resources of the RWTH Rechenzentrum, as well as the funding provided by the DFG (German Science Foundation) within the collaborative research center SFB 917 Nanoswitches. W. Zhang acknowledges DAAD and CSC for financial support.

References

1. Wuttig M, Yamada N (2007) Nature Mater 6:824
2. Lencer D, Salinga M, Wuttig M (2011) Adv Mater 23:2030
3. Wright CD, Liu Y, Kohary KI, Aziz MM, Hicken RJ (2011) Adv Mater 23:3408
4. Song WD, Shi LP, Miao XS, Chong CT (2008) Adv Mater 20:2394
5. Li Y, Mazzarello R (2012) Adv Mater 24:1429
6. Zhang W, Ronneberger I, Li Y, Mazzarello R (2012) Adv Mater 24:4387
7. Kolobov AV, Fons P, Frenkel AI, Ankudinov AL, Tominaga J, Uruga T (2004) Nature Mater 3:703
8. Baker DA, Paesler MA, Lucovsky G, Agarwal SC, Taylor PC (2006) Phys Rev Lett 96:255501
9. Kohara S, Kato K, Kimura S, Tanaka H, Usuki T, Suzuya K, Tanaka H, Moritomo Y, Matsunaga T, Yamada N, Tanaka Y, Suematsu H, Takata M (2006) Appl Phys Lett 89:201910
10. Klein A, Dieker H, Späth B, Fons P, Kolobov AV, Steimer C, Wuttig M (2008) Phys Rev Lett 100:016402
11. Shportko K, Kremers S, Woda M, Lencer D, Robertson J, Wuttig M (2008) Nature Mater 7:653
12. Siegrist T, Jost P, Volker H, Woda M, Merkelbach P, Schlockermann C, Wuttig M (2011) Nature Mater 10:202
13. Njoroge WK, Wuttig M (2001) J Appl Phys 90:3816
14. Matsunaga T, Akola J, Kohara S, Honma T, Kobayashi K, Ikenaga E, Jones RO, Yamada N, Takata M, Kojima R (2011) Nature Mater 10:129
15. Caravati S, Bernasconi M, Kühne TD, Krack M, Parrinello M (2007) Appl Phys Lett 91:171906
16. Akola J, Jones RO (2007) Phys Rev B 76:235201
17. Akola J, Jones RO (2008) Phys Rev Lett 100:205502
18. Lencer D, Salinga M, Grabowksi B, Hickel T, Neugebauer J, Wuttig M (2008) Nature Mater 7:972
19. Mazzarello R, Caravati S, Angioletti-Uberti S, Bernasconi M, Parrinello M (2010) Phys Rev Lett 104:085503
20. Sosso GC, Caravati S, Mazzarello R, Bernasconi M (2011) Phys Rev B 83:134201
21. Caravati S, Colleoni D, Mazzarello R, Kühne TD, Krack M, Bernasconi M, Parrinello M (2011) J Phys Condens Matter 23:265801
22. Zhang W, Thiess A, Zalden P, Zeller R, Dederichs PH, Raty J-Y, Wuttig M, Bluegel S, Mazzarello R (2012) Nature Mater 11:952
23. van Pieterson L, Lankhorst MHR, van Schijndel M, Kuiper AET, Roosen JHJ (2005) J Appl Phys 97:083520
24. Caravati S, Bernasconi M, Parrinello M (2010) Phys Rev B 81:014201
25. Thonhauser T, Scheidemantel TJ, Sofo JO, Badding JV, Mahan GD (2003) Phys Rev B 68:085201
26. Raoux S, Wuttig M (eds) (2008) Phase change materials: science and applications. Springer, Berlin
27. Medvedev NN, Voloshin VP, Luchnikov VA, Gavrilova ML (2006) J Comput Chem 27:1676
28. SMS Group at the Institute of Chemical Kinetics and Combustion, SB RAS (2006) Calculation of the Voronoi S-network (additively weighted Voronoi diagram). http://www.kinetics.nsc.ru/sms/?Software:VNP
29. Kühne TD, Krack M, Mohamed FR, Parrinello M (2007) Phys Rev Lett 98:066401
30. VandeVondele J, Krack M, Mohamed F, Parrinello M, Chassaing T, Hutter J (2005) Comput Phys Commun 167:103
31. CP2K homepage. http://www.cp2k.org
32. Perdew JP, Burke K, Ernzerhof M (1996) Phys Rev Lett 77:3865
33. Goedecker S, Teter M, Hutter J (1996) Phys Rev B 54:1703